

Morphology and conductivity improvement of metal mesh through roll-to-roll-compatible near-infrared sintering

Li-Wen Wang¹, Cheng-Yao Lo^{1,2} ✉

¹*Institute of NanoEngineering and MicroSystems, National Tsing Hua University, Hsinchu 30013, Taiwan*

²*Department of Power Mechanical Engineering, National Tsing Hua University, Hsinchu 30013, Taiwan*

✉ E-mail: chengyao@mx.nthu.edu.tw

Published in Micro & Nano Letters; Received on 10th June 2017; Revised on 8th August 2017; Accepted on 22nd August 2017

This work proposes a near-infrared (NIR) sintering method to improve the surface roughness and to reduce the sheet resistance of a gravure-offset-printed metal mesh with a viscous silver paste that contains large nanoparticles. Results indicate that the sintering was thorough because the porosity in the metal mesh approached 0%. Examination proved a 29.7% surface roughness improvement in the metal mesh after NIR sintering, which outperformed the conventional oven operations by 2.37%. In addition, material analyses through both energy-dispersive and Raman spectroscopy explained the reduction of insulative elements and features with chemical bonds in the metal mesh, supporting the finding of the most significant improvements in surface roughness (90.9%) and sheet resistance (98.6%). The effective NIR sintering evaluated in this work was proven to be not only capable of replacing discontinuous oven operations in roll-to-roll manufacturing but also efficient in enhancing the material characteristics under identical sintering conditions compared with conventional oven operations.

1. Introduction: In the development of display devices, increasing the illumination efficiency of organic light emitting diodes (OLEDs) is important. To this end, one of the most promising solutions is to improve the conductivity of the anode. Among practical proposals, a metal mesh fabricated atop or in lieu of transparent conducting oxides, such as indium tin oxide (ITO), have been found effective [1–3] on conductivity improvement. In addition, because manufacturers are keen to fabricate not only specific individual layers but also the complete OLED structure cost-efficiently, roll-to-roll (R2R) manufacturing with different printing steps is considered practical [4–6]. Take OLED as an example, the use of silver (Ag) paste with nanoparticles as part of its anode – specifically, as a metal mesh – has been extensively evaluated using various printing methods [7, 8]. Besides OLEDs, metal mesh can also be used in other applications that have to take both electrical and optical performance of electrodes into considerations.

Metal mesh not only improves the conductivity of the anode but also exhibits high transmittance, thus supporting display applications. However, large nanoparticles (> 300 nm on average) have been preferred in the viscous (> 10000 cP) Ag paste considering cost, preparation simplicity, and electrical conductivity. Consequently, the as-printed metal mesh would usually exhibit poor surface roughness because of the large nanoparticles, resulting in concerns about the OLED reliability because each layer in an OLED is usually thinner than few tens of nanometres. Fortunately, the surface roughness of the metal mesh could be alleviated by sintering, because thermal energy would not only melt but also reshape the nanoparticles, improving the surface flatness [9]. Nevertheless, studies on sintering and its effectiveness on printed Ag inks have only examined low-viscosity (< 20 cP) and small nanoparticles (< 100 nm in average), and sintering for large nanoparticles is yet to be evaluated. Developing effective and R2R-compatible sintering methods are essential to alleviate the surface roughness of printed viscous Ag paste with large nanoparticle size.

Near-infrared (NIR), in which thermal energy delivery depends not only on conduction but also radiation, was previously proven to be both R2R-compatible and sintering-efficient [10]. Accordingly, in this Letter, applying NIR on the printed metal mesh was proposed for sintering large nanoparticles in viscous

Ag paste. The NIR used in this Letter was although an individual module that was not yet integrated into a system, it supports continuous manufacturing when it is mounted to an R2R production line (Fig. 1).

To ensure complete sintering in the metal mesh, material investigations were conducted to examine the porosity, elemental content, and chemical bonds between various elements. The surface roughness improvement and enhanced electrical characteristics of the metal mesh were confirmed by examining the surface morphology and sheet resistance (R_s), respectively. In addition to the morphological and material analyses, the process development of various sintering conditions was studied to achieve identical sheet resistance and optical transmittance in the metal mesh through figure-of-merit (FOM), and solutions for R2R manufacturing that surpass the limits of current R2R equipment were realised.

2. Process: The metal mesh was designed and patterned onto ITO glass through R2R gravure-offset printing, in which ITO covered the complete glass with 15 Ω /sq sheet resistance and 500 nm thickness. The paste was composed of Ag (90 wt%) nanoparticles, resins (5 wt%), and solvents (5 wt% dipropylene glycol monomethyl ether), in which the Ag nanoparticles averaged 300 nm in diameter. The metal mesh printed on the ITO glass had a 30 μ m line width and 380 μ m line pitch. Immediately after printing, the sample (baseline) was sent to a customised oven (a separated tool from the R2R) for sintering for 30 min at 150°C in atmospheric air. In addition, several as-printed samples were sintered using the proposed NIR system (Adphos, NIR42 – 125) for up to 1800 s under an exposure intensity of 1500 kW/m². Because the sample (30 mm × 30 mm) was placed under and close to the NIR emitter (Fig. 1), which was 125 mm long and 42 mm wide, the exposure ensured uniform radiation and temperature distribution on the sample. By adjusting the distance between the NIR emitter and the sample, the samples were exposed to 150–600°C.

In addition to the NIR approach, wherein the process temperature was limited using its exposure intensity, a customised furnace system was also introduced in this Letter to simulate realisable process temperatures using NIR. The furnace supports thermal treatment of samples at 600–900°C for up to 1800 s, bridging the drawbacks of currently available NIR approaches. In practise,

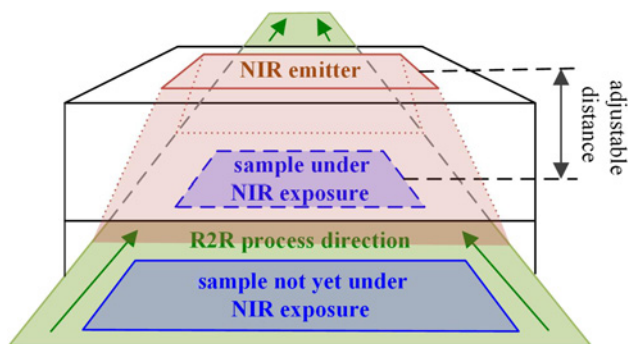


Fig. 1 Schematic plot of an integrated NIR module in a R2R system

with the introduction of an appropriate NIR apparatus, which was not available in this Letter, these operation temperatures are realisable [11].

Because one purpose of developing effective sintering methods for the metal mesh is to suppress its surface roughness, the surface morphology of the metal mesh was characterised using a surface profiler (Bruker, Dektak XT). For each sample, nine scans were performed at various locations of the metal mesh, with the average value (R_a) of the complete scan (50 μm under 3 mg force at 5 $\mu\text{m/s}$) indicating the surface roughness of the sample.

To observe sintering efficiency, a scanning electron microscope (SEM) was used to examine the cross-sectional structure of the metal mesh with a covering layer of platinum (Pt) to enhance the contrast between Ag and the substrate (ITO on glass). The porosity of the metal mesh was quantified with the help of image operation [12–15] and less porosity in the metal mesh implies higher sintering efficiency.

The samples were exposed to atmospheric air during NIR sintering. Although the oven and furnace had relatively closed systems, in which atmospheric air is enclosed in the chamber, the interactions between Ag and other elements in atmospheric air, remaining resin, or solvent make negative contributions regarding the sheet resistance of the metal mesh. To identify the composition of the metal mesh, energy-dispersive spectroscopy (EDS; Oxford Instrument, Aztec) and Raman spectroscopy (Horiba Jobin Yvon, LabRAM HR 800UV) were introduced to examine the elemental content and chemical bonds between the various elements, respectively.

In addition to the physical and material analysis, scientific judgment that considered both the electrical and optical behaviours of the metal mesh was conducted through the FOM method [16]

$$T = [1 + (188.5/(R_s \text{FOM}))]^{-2},$$

where T is the average transmittance in the visible region. Because thin films exhibit high optical transmittance but low electrical conductivity, an improvement in one of these parameters leads to the degradation of the other. The introduction of FOM not only simultaneously considers both quantities but also provided solution varieties in the process development, as described later.

3. Results

3.1. Surface roughness and sheet resistance: Because the average Ag nanoparticle size is 300 nm, the as-printed sample exhibited a poor R_a of 174.9 nm. With identical thermal sintering at 150°C for 30 min, the R_a noticeably reduced to 126.4 nm (27.7% improvement) and 123.0 nm (29.7% improvement) when processed using the oven and NIR, respectively (Fig. 2). This result implied that the Ag nanoparticles on the surface of the metal mesh were sintered and the R_a was improved by the connection of the Ag nanoparticles, regardless of the structure underneath the surface. Although higher sintering temperatures

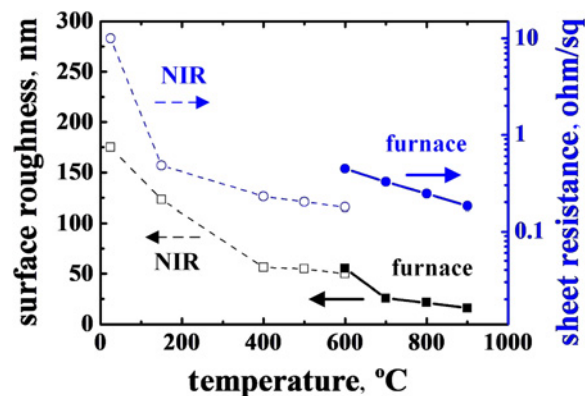


Fig. 2 Surface roughness and sheet resistance of samples sintered using NIR and the furnace at various temperatures

were not designed for the baseline (oven) process, which was also limited by the process capability, raising the sintering temperature for NIR showed continuous R_a improvement. To evaluate the possibility of further suppressing R_a at temperatures exceeding 600°C, a furnace was used for sintering. The result indicates a continuous suppression of R_a from 25.7, 21.5, and 15.9 nm at 700, 800, and 900°C, respectively.

From the results, one can conclude that NIR, compared with the oven, made a similar contribution to R_a improvement. However, the electrical performance of the metal mesh as examined using R_s implies that NIR surpasses the oven in terms of the sintering efficiency. As indicated in Fig. 2, R_s noticeably reduced from 9.93 to 1.00 and 0.48 Ω/sq for the oven- and NIR-sintered sample, respectively. Although the difference in R_s improvements in the two methods is minor (89.9% for the oven and 95.2% for NIR), the final R_s improvement through NIR sintering was 52% higher than that through oven sintering. This implied that not only could NIR replace ovens to support R2R processes, but that an efficient NIR sintering mechanism exists.

In addition, when the process temperature was continuously raised, R_a and R_s were, respectively, reduced to 56.3 nm and 0.23 Ω/sq through NIR sintering at 400°C. Similarly, when the process temperature was also continuously raised, R_s was, respectively, reduced to 0.33, 0.24, and 0.18 Ω/sq through furnace sintering at 700, 800, and 900°C. These results prove that high thermal energy continuously improved both the surface morphologies and the electrical characteristics of the metal mesh.

3.2. Structure and porosity: Cross-sectional SEM pictures showed that the as-printed Ag nanoparticles were not only sparsely distributed in the metal mesh (Fig. 3a) but also disconnected from each other. Nevertheless, although the oven-sintered sample showed connected Ag nanoparticles (Fig. 3b) in the metal mesh, porosity still remained high (28.39%) and did not show a noticeable improvement from the as-printed sample (32.95%). In addition, individual Ag nanoparticles were still observable in the oven-sintered sample, but the NIR-sintered sample showed connected Ag nanoparticles without any isolated individuals (Fig. 3c). The porosity in the metal mesh noticeably reduced to 13.86% in the NIR-sintered sample. Compared with its oven-sintered counterpart, the NIR-sintered metal mesh exhibited a 57.9% porosity improvement from the as-printed sample. Because NIR sintered the Ag nanoparticles through both radiation and conduction, it effectively and efficiently sintered Ag nanoparticles, not only on the surface but also inside the metal mesh. However, the Ag nanoparticles did not show a distinguishable size difference along the depth of the metal mesh.

To evaluate the requirement for the complete sintering of the Ag nanoparticles in the metal mesh, the NIR temperature was

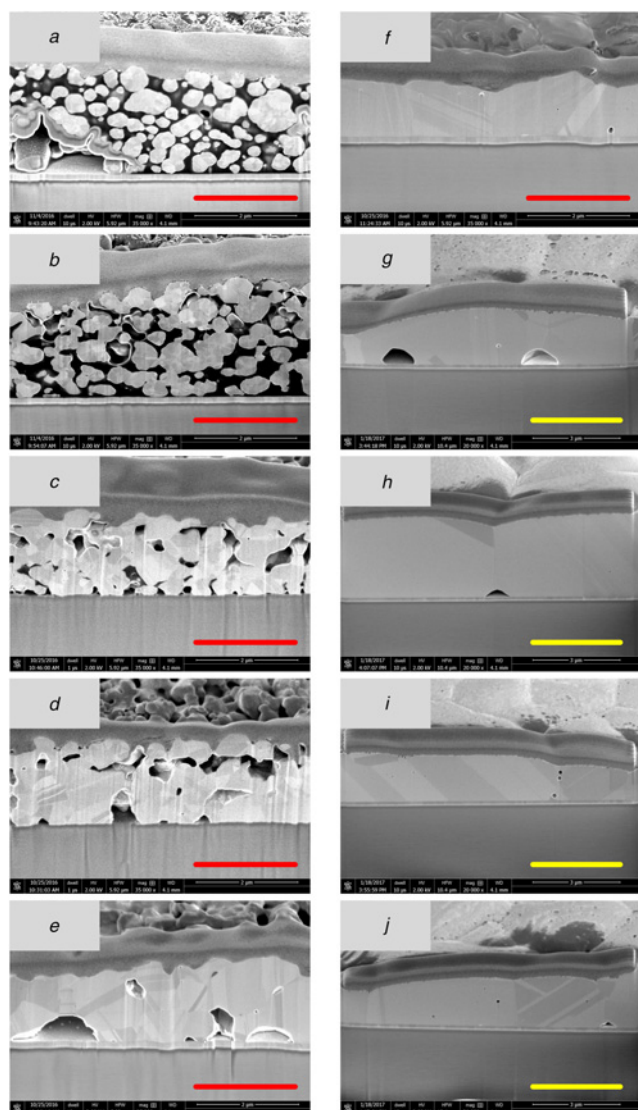


Fig. 3 SEM images of the sample
 a As-printed and sintered using
 b Oven at 150°C
 c NIR at 150°C
 d NIR at 400°C
 e NIR at 500°C
 f NIR at 600°C
 g Furnace at 600°C
 h Furnace at 700°C
 i Furnace at 800°C, and
 j Furnace at 900°C. Scale bars in (a)–(f) and in (g)–(j) are 2 and 3 μm , respectively. Note that the materials from the bottom to the top were sequentially glass, ITO, Ag (paste), and Pt

sequentially raised while the sintering duration was maintained at 30 min. SEM examinations revealed that the porosity was gradually reduced to nearly 0% when the process temperature finally reached 600°C (Figs. 3d–f), indicating thorough sintering. With the porosity reduction, R_s also reduced proportionally (Fig. 2). Aside from the NIR, the furnace also indicated a thorough sintering with porosity close to 0% when the temperature exceeded 800°C for identical process duration (Figs. 3g–j).

The theoretical melting point of Ag nanoparticles of size 300 nm is $\sim 900^\circ\text{C}$ [17]. However, although the average nanoparticle size of Ag paste in this Letter was 300 nm, the presence of many smaller nanoparticles (Fig. 3a) could help on lowering the overall effective melting point. Consequently, the metal mesh was completely sintered under the conditions used in this Letter.

3.3. Element composition: R_s improvement using NIR and furnace could be attributed not only to complete sintering of connections between Ag nanoparticles but also to the increased content of conducting Ag. EDS results show that the Ag content in the as-printed, oven-, and NIR-sintered samples was 69.9, 72.6, and 72.1%, respectively (Figs. 4a–c). Although their Ag content was similar, the oxygen (O) content varied in the samples processed using the oven (10.3%) and NIR (6.1%). The remarkable suppression of oxygen content in the NIR-sintered sample implies improved electrical characteristics by efficient energy delivery to the complete metal mesh despite the NIR operations being conducted in atmospheric air. Compared with the as-printed sample, the Ag and O content in the NIR-sintered samples was increased and suppressed (Figs. 4c and d), and the improvement of the as-printed characteristics were 5.29 and 50% at 600°C (Fig. 4d), respectively. By contrast, although the carbon (C) content remained high at various NIR temperatures (Figs. 4c and d), its variation was small. Taking both minor C increment and major O reduction by NIR sintering into consideration, the electrical behaviour of the metal mesh was improved.

For the furnace-sintered samples, the Ag content was, respectively, 66.6, 69.9, and 74.5% at 700, 800, and 900°C; the corresponding carbon content was 22.9, 21.6, and 16.2%, and the corresponding oxygen content was 10.5, 8.5, and 9.3%. Compared with the as-printed sample, the Ag content in the furnace-sintered samples further increased, and the improvement reached 6.5% at 900°C (Fig. 4e). These improvements in Ag content explain the R_s improvement observed in this Letter (Fig. 2). In addition, NIR delivers thermal energy through both radiation and conduction, outperforming the oven and furnace. Consequently, even higher Ag content ($> 74.5\%$) in the metal mesh can be expected when suitable NIR apparatus is available for temperatures up to 900°C.

The chemical bonds between the different elements in the metal mesh were analysed through Raman spectroscopy. The broad peak centred at 255 cm^{-1} was associated with silver carbonate (Fig. 5) [18–20]. With raised sintering temperatures, the silver carbonate decomposed, and carbon and oxygen were expelled to the atmospheric environment regardless of the sintering method. This result also supported previous analysis of the elemental content.

Furthermore, a noticeable peak appeared at 485 cm^{-1} . This peak, which was stronger in the NIR-sintered samples than in the others, was associated with silver oxide [11, 12]. Because only NIR sintering was conducted in an oxygen-rich environment, the sample sintered using NIR at 150°C showed a remarkable peak. Nevertheless, under higher NIR sintering temperatures (400°C), the silver oxide also decomposed, and the oxygen was expelled to the atmospheric environment [21], showing a relatively negligible peak at 485 cm^{-1} . By contrast, the oven and furnace sintering were conducted in an enclosed environment, where the atmospheric air was consumed and not continuously supplied during operation, avoiding extensive silver oxide generation. Raman spectroscopy analysis indicated that the high sintering temperature and enclosed environment would be helpful for suppressing the existence of insulative materials after sintering, which in turn implies an improvement in the electrical characteristics in the metal mesh.

4. Discussion: One advantage of using metal mesh in the anodes of display applications such as OLEDs is the acceptable optical transmittance. The experimental results show that the transmittance of the metal mesh is gradually reduced by $\sim 15\%$ (Fig. 6) after 30 min of furnace sintering. Although disadvantageous, this transmittance degradation usually accompanies advantageous electrical conductivity improvement [22–24]. Because electrical conductivity is negatively related to transmittance, a fair comparison requires considering these two characteristics simultaneously. In various studies, FOM was introduced not only to evaluate both characteristics at the same

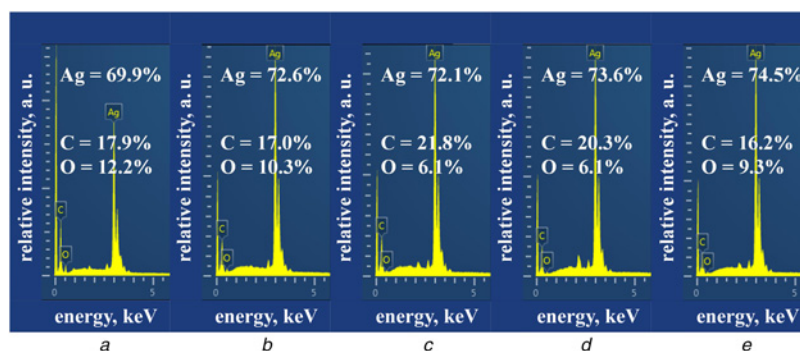


Fig. 4 EDS analysis result of the sample

a As-printed and sintered using

b An oven at 150°C

c NIR at 150°C

d NIR at 600°C

e Furnace at 900°C

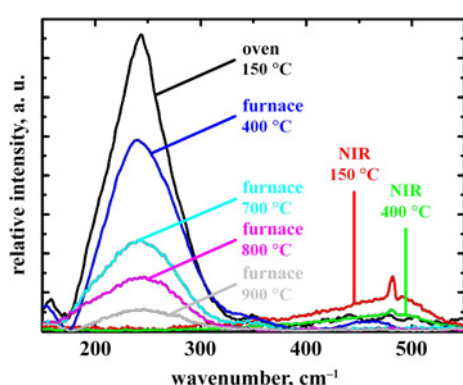


Fig. 5 Raman spectra of samples sintered under various methods and conditions

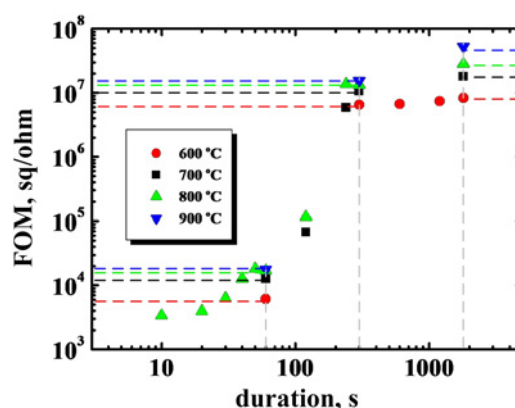


Fig. 7 FOM for samples sintered under various furnace conditions

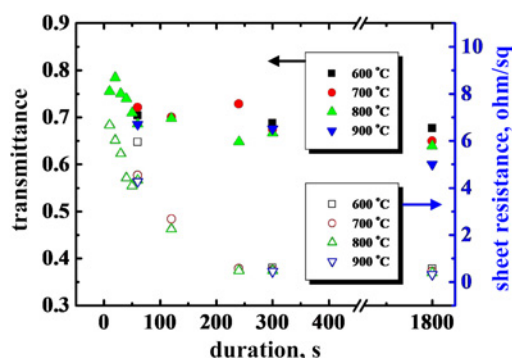


Fig. 6 Transmittance and sheet resistance for samples sintered under various furnace conditions

time but also to find an optimised process condition [25]. Because this Letter finds both sintering temperature and duration influence the surface roughness and sheet resistance improvements, sintering conditions were altered to evaluate the FOMs of the furnace-sintered samples.

The results indicate that the transmittance of the metal mesh was reduced at corresponding sintering conditions if low sheet resistances were expected (Fig. 6). These findings are in accordance with results from the literature on transparent conducting structures, regardless of the materials used [22–24]. A continuous enlarging FOM appeared at either fixed sintering temperatures with prolonged

sintering duration or fixed sintering duration but raised the temperature (Fig. 7). Although the FOM evaluation implies that the optimisation of the sintering procedure of furnace was not achieved in this Letter, it nevertheless provides several combinations of sintering temperatures and durations. For example, if a specific FOM is required with limited temperature supportiveness from the sintering system, a prolonged sintering duration would be helpful. Conversely, when sintering duration is considered critical in an R2R manufacturing, the sintering temperature can be raised for an identical FOM.

5. Conclusion: This work proposed and evaluated R2R-compatible NIR sintering and the characteristics of gravure-offset-printed metal mesh. Morphological surface roughness, electrical sheet resistance, and optical transmittance of the samples were comprehensively examined. Because NIR delivers thermal energy through both radiation and conduction, viscous Ag paste with large nanoparticles was sintered with improved surface roughness compared with its counterpart thermally sintered by a conventional non-R2R-compatible oven under identical sintering temperature and duration. Material analysis through EDS proved that the Ag content in the NIR-sintered metal mesh increased by 0.69% when the conditions were identical to that of the oven sintering, indicating a significant 95.2% enhancement of the sheet resistance in the metal mesh.

In summary, the NIR sintering of viscous Ag paste with large nanoparticles was proved effective. The efficient improvement on the morphological and electrical characteristics of the metal mesh makes R2R-compatible NIR sintering to replace conventional

non-R2R-compatible oven sintering possible, potentially enabling the continuous printing and fabrication of display applications such as OLEDs. Although the sintering duration used in this Letter was long with the individual NIR module, it could be significantly shortened if advanced NIR apparatus with sufficiently strong exposure intensity becomes available. We believe that with a proper arrangement such as a mounted NIR module in a continuous R2R production line, further investigations on the performance of OLED or other display applications could be conducted in the future.

6. Acknowledgments: This study was partially supported by the Ministry of Science and Technology (grant nos. MOST104-2628-E-007-005-MY2 and MOST106-2221-E-007-051), Taiwan, and by the ‘Toward World-Class University Project’ of National Tsing Hua University (grant no. 106N523CE1). The authors were grateful for access to the facilities at the Center for Nanotechnology, Materials Science, and Microsystems of National Tsing Hua University (NTHU), which was partly supported by the Ministry of Science and Technology. In this work, some of the NIR processes were supported by MOS Technology Inc., and the gravure-offset printing was supported by the Industrial Technology Research Institute. The authors also thank Dr. Nyan-Hwa Tai and his group in the Department of Material Science and Engineering, NTHU for the Raman spectroscopy analysis.

7 Reference

- [1] Kang M.G., Guo L.J.: ‘Semitransparent Cu electrode on a flexible substrate and its application in organic light emitting diodes’, *J. Vac. Sci. Technol. B*, 2007, **25**, pp. 2637–2641
- [2] Granqvist C.G., Hultaker A.: ‘Transparent and conducting ITO films: new developments and applications’, *Thin Solid Films*, 2002, **411**, pp. 1–5
- [3] Kang M.G., Guo L.J.: ‘Nanoimprinted semitransparent metal electrodes and their application in organic light-emitting diodes’, *Adv. Mater.*, 2007, **19**, pp. 1391–1396
- [4] Sowade E., Kang H., Mitra K.Y., *ET AL.*: ‘Roll-to-roll infrared (IR) drying and sintering of an inkjet-printed silver nanoparticle ink within 1 s’, *J. Mater. Chem. C*, 2015, **3**, pp. 11815–11826
- [5] Hwang H.J., Oh K.H., Kim H.S.: ‘All-photonic drying and sintering process via flash white light combined with deep-UV and near-infrared irradiation for highly conductive copper nano-ink’. Scientific Reports, 2016, vol. **6**, 19696
- [6] Søndergaard R.R., Hösel M., Krebs F.C.: ‘Roll-to-roll fabrication of large area functional organic materials’, *Polym. Phys.*, 2013, **51**, pp. 16–34
- [7] Laurent M.S., Razali M.A., Christopher A.M., *ET AL.*: ‘Silver grid transparent conducting electrodes for organic light emitting diodes’, *Org. Electron.*, 2014, **15**, pp. 3492–3500
- [8] Michael L., Shlomo M.: ‘Flexible transparent conductive coatings by combining self-assembly with sintering of silver nanoparticles performed at room temperature’, *J. Mater. Chem.*, 2011, **21**, pp. 15378–15382
- [9] Hösel M., Krebs F.C.: ‘Large-scale roll-to-roll photonic sintering of flexo printed silver nanoparticle electrodes’, *J. Mater. Chem.*, 2012, **22**, pp. 15683–15688
- [10] Perelaer J., Schubert U.S.: ‘Novel approaches for low temperature sintering of inkjet-printed inorganic nanoparticles for roll-to-roll (R2R) applications’, *J. Mater. Res.*, 2013, **28**, pp. 564–573
- [11] Martyn C., Tim C.C., Davide D., *ET AL.*: ‘Ultrafast near-infrared sintering of a slot-die coated nano-silver conducting ink’, *J. Mater. Chem.*, 2011, **21**, pp. 7562–7564
- [12] Mark A., Jaakko L., Marja V., *ET AL.*: ‘Substrate-facilitated nanoparticle sintering and component interconnection procedure’, *Nanotechnology*, 2010, **21**, p. 475204
- [13] Shlomo M., Michael G., Alexander K.: ‘Copper nanoparticles for printed electronics: routes towards achieving oxidation stability’, *Materials*, 2010, **3**, pp. 4626–4638
- [14] Hu A., Guo J.Y., Alarifi H., *ET AL.*: ‘Low temperature sintering of Ag nanoparticles for flexible electronics packaging’, *Appl. Phys. Lett.*, 2010, **97**, p. 153117
- [15] Chan H.J., Huang B.C., Wang L.W., *ET AL.*: ‘Porosity reduction in inkjet-printed copper film by progressive sintering on nanoparticles’, *Thin Solid Films*, 2017, **627**, pp. 33–38
- [16] Hu L., Hecht D.S., Grüner G.: ‘Percolation in transparent and conducting carbon nanotube networks’, *Nano Lett.*, 2004, **4**, pp. 2513–2517
- [17] Anna M., Albert G.N., Esko I.K.: ‘The role of metal nanoparticles in the catalytic production of single-walled carbon nanotubes’, *J. Phys., Condens. Matter*, 2003, **15**, pp. 3011–3035
- [18] Geoffrey I.N., Graham A.B., James B.M.: ‘Oxygen chemisorption on an electrolytic silver catalyst: a combined TPD and Raman spectroscopic study’, *Appl. Surf. Sci.*, 2003, **214**, pp. 36–51
- [19] Hiroshi N., Hu Z.M., Hiromi N., *ET AL.*: ‘Activation of O₂ on Cu, Ag, and Au surfaces for the epoxidation of ethylene: dipped adcluster model study’, *Surf. Sci.*, 1997, **387**, pp. 328–341
- [20] Wang C.B., Goutam D., Israel E.W.: ‘Interaction of polycrystalline silver with oxygen, water, carbon dioxide, ethylene, and methanol: in situ Raman and catalytic studies’, *J. Phys. Chem. B*, 1999, **103**, pp. 5645–5656
- [21] Carlisle C.I., Fujimoto T., Sim W.S., *ET AL.*: ‘Atomic imaging of the transition between oxygen chemisorption and oxide growth on Ag {1 1 1}’, *Surf. Sci.*, 2000, **470**, pp. 15–31
- [22] Sergio B.S., Sylvain G.C.: ‘Figures of merit for high-performance transparent electrodes using dip-coated silver nanowire networks’, *J. Nanomaterials*, 2012, **2012**, p. 286104
- [23] Lee J.Y., Stephen T.C., Cui Y., *ET AL.*: ‘Solution-processed metal nanowire mesh transparent electrodes’, *Nano Lett.*, 2008, **8**, pp. 689–692
- [24] Jorik G., Pierpaolo S., Albert P.: ‘Transparent conducting silver nanowire networks’, *Nano Lett.*, 2012, **12**, pp. 3138–3144
- [25] Zhou Y.X., Hu L.B., Grüner G.: ‘A method of printing carbon nanotube thin films’, *Appl. Phys. Lett.*, 2006, **88**, p. 123109